STRUCTURAL BIOLOGY COMMUNICATIONS

ISSN 2053-230X

Structural themes of cereblon-recruiting degraders: selected recent examples

Sana Ahmed* and Michael Rowley

Department of Biochemistry and Molecular Biology, University of British Columbia, Vancouver, BC V6T 1Z3, Canada. *Correspondence e-mail: sana2000@student.ubc.ca

Received 31 July 2026
Accepted 19 October 2026

Edited by M. J. van Raaij, Centro Nacional de Biotecnología – CSIC, Spain

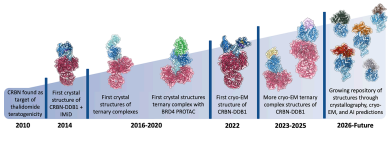
This article is part of Celebrating 20 Years of *Acta Crystallographica Section F*.

Keywords: structural biology; cryo-EM; X-ray crystallography; molecular-glue degraders; PROTACs; cereblon; structure-based drug design.

Targeted protein degradation is orchestrated by interactions between target proteins and components of the ubiquitin–proteasome system such as the E3 ligase cereblon. Advances in molecular visualization of the target complexes formed by cereblon have provided insights into how cereblon, degrader molecules and drug-induced non-native targets come together to enable cellular breakdown. Here, we review selected examples demonstrating how X-ray crystallography and cryogenic-electron microscopy (cryo-EM) have been applied to cereblon structures to guide the development and validation of novel preclinical heterobifunctional and molecular-glue degraders. In some instances, cryo-EM and X-ray crystallography enabled structure-guided optimization of degrader potency, while in others structural insights elucidated the molecular mechanisms underlying target specificity. Collectively, these structural studies are improving the reliability of computational predictions and paving the way for more structure-based design of cereblon-recruiting small-molecule degraders.

1. Introduction

The use of thalidomide to treat morning sickness in the late 1950s and early 1960s resulted in a devastating public health tragedy, with more than 120 000 reported (and thousands more predicted) cases of stillbirths, miscarriages and birth defects. The teratogenic effects of thalidomide were subsequently linked to its interaction with cereblon (CRBN), a molecular target identified years later (Ito *et al.*, 2010). Thalidomide was a mimic of a naturally occurring biological degron, cyclic imides, formed on the aging of proteins that CRBN engages, resulting in ubiquitination and proteolytic degradation of the aged protein (Xu & Woo, 2025). Upon thalidomide binding, CRBN undergoes a tertiary conformational change, making it amenable to off-target binding and degradation of proteins such as the developmentally important spalt-like transcription factor 4 (SALL4) and isoforms of p63 (Matyskiela *et al.*, 2018; Asatsuma-Okumura *et al.*, 2019). This discovery ignited interest in CRBN biology and the idea that CRBN-recruiting compounds, including molecular-glue degraders (MGDs) and heterobifunctional degraders/PROteolytic TArgeting Chimeras (PROTACs), could be designed against novel targets to induce degradation (Békés *et al.*, 2022). Heterobifunctional degraders are usually composed of bivalent chemical moieties to recruit the target protein and the E3 ligase through rational design, while MGDs are monovalent compounds that are usually discovered through high-throughput screening. Targeted protein degradation is now a multi-billion dollar industry, with CRBN as one of the core degradation-inducing modalities for several chemical entities in the clinical pipeline for treatment of a myriad of



OPEN ACCESS
Published under a CC BY 4.0 licence

diseases, including Vepdegestrant, the first FDA-approved PROTAC as of May 2026 (Campone *et al.*, 2025). In this review, we highlight how structural biology is beginning to make important contributions to help catalyze both the discovery of small-molecule degraders and an improved understanding of the underlying structural mechanisms.

1.1. Background to CRBN-mediated protein degradation

In cells, CRBN performs E3-ligase-independent functions but most commonly functions as the substrate receptor of the E3 ligase Cullin–RING ligase 4 (CRL4) complex that cooperatively binds and ubiquitinates target proteins (Stewart *et al.*, 2016). CRL4 complexes use CRBN to recognize and tether substrates so that the E2–ubiquitin transferase enzyme proximal to CRBN can transfer ubiquitin to lysine residues on the CRBN-bound target protein. Following extension of the polyubiquitin chain, the substrate dissociates from the CRL4 complex and is subsequently degraded by the proteasome.

CRBN is a highly dynamic protein that undergoes a large conformational change upon engagement of the thalidomide-binding domain, either by a degrader (Fischer *et al.*, 2014) or by a protein post-translationally modified with a CRBN-specific degron which includes a C-terminal cyclic imide [cyclic asparagine (cN) and cyclic glutamine (cQ)] (Xu & Woo, 2025). Following binding, CRBN can bind a host of degrader-induced non-native or native targets, forming a broad protein–protein interaction interface with the target through induced proximity, earning these degraders the title of molecular-glue degraders (MGDs; Ito *et al.*, 2010). Thalidomide, pomalidomide and lenalidomide all recruit similar targets to CRBN, including IKZF1 (Ikaros), IKZF3 (Aiolos), SALL4 and casein kinase 1 alpha (CK1α; Donovan *et al.*, 2018; Matyskiela *et al.*, 2018, 2020; Petzold *et al.*, 2016). Once bound, the targets can be ubiquitinated and subsequently degraded. While many CRBN-bound targets are marked for degradation, their mode of binding to CRBN is unique.

1.2. Timeline of structural insights into CRBN biochemistry

CRBN (UniProt Q96SW2; UPID UP000005640) is composed of three domains: the N-terminal domain, Lon, a helical bundle domain (HBD) interacting with damage-specific DNA-binding protein 1 (DDB1), and a C-terminal domain which binds to thalidomide and analogs (also known as the thalidomide-binding domain; TBD) (Fig. 1*a*). The first high-resolution crystal structures of CRBN were reported in 2014 (Chamberlain *et al.*, 2014; Fischer *et al.*, 2014). Determined at a resolution of 3.0–3.5 Å, these structures revealed human CRBN and *Gallus gallus* DDB1 in complex with the orthosteric ligands thalidomide, pomalidomide and lenalidomide. Each structure showed the degrader molecule bound to the thalidomide-binding domain in a hydrophobic pocket lined with three key tryptophan residues (Trp380, Trp386 and Trp400) that became known as the Tri-trp pocket (Figs. 1*a* and 1*b*).

While the structures did not capture CRBN bound to a target protein, Fischer *et al.* (2014) performed mutagenesis analysis revealing that the C-terminus of CRBN is likely to be involved in target binding. It was not until three years later that the first structure of CRBN in complex with thalidomide and a target, IKZF1, was determined (Sievers, Petzold *et al.*, 2018). These structures confirmed the previous hypotheses that the thalidomide-binding domain serves as the primary protein–target binding site and enabled the identification of the target-binding footprint (Fig. 1*b*). IKZF1 made contacts with both CRBN and thalidomide via its zinc-finger motif. However, a recurring structural feature among CRBN targets is a β-hairpin loop containing a conserved glycine residue, commonly referred to as the canonical G-loop motif. This was structurally validated by several follow-up studies determining the crystal structures of unique CRBN–degrader–target complexes, including CRBN–CC-885–GSPT1 (Matyskiela *et al.*, 2016), CRBN–lenalidomide–CK1α (Petzold *et al.*, 2016) and CRBN–pomalidomide–SALL4 (Matyskiela *et al.*, 2020). All unique structures share a similar binding pose of the degrader glutarimide moiety with variations observed in the binding footprint of the target, as also reflected in the studies reviewed here (Fig. 1*c*).

Subsequent structural studies of heterobifunctional degraders targeting bromodomain 1 of BRD4 expanded the target and structural landscape of CRBN-recruiting degraders while challenging conventional assumptions about the cooperativity required for ternary-complex formation (Nowak *et al.*, 2018). These studies demonstrated the various ways that CRBN can be harnessed for therapeutic potential, yet a mechanistic understanding of the conformational dynamics of CRBN remained elusive. A major contribution towards this was reported by Watson *et al.* (2022), who used cryogenic-electron microscopy (cryo-EM) to show that CRBN can adopt two distinct conformations: an apo (open) state and a degrader-bound (closed) state (Fig. 1*b*). Before binding to a cyclic imide-containing molecule, the Lon and thalidomide-binding domains are positioned 51° from each other in the open state. Cyclic imide binding to the tri-Trp pocket induces a hinge-like motion between the protein domains, reducing the separation to 31°. This motion induces a concerted movement of the sensor loop (amino acids 341–361) with restructuring of the protein backbone. In addition to the changes in the tertiary structure of cereblon, the cryo-EM structures revealed different conformations of the β-propellor B (BPB) domain of DDB1 that contributed to accommodation in the CRL4 ligase, and a distribution of open and closed states based on the respective degraders. These studies have led to a rapid expansion in the number of cryo-EM structures of CRBN bound to degraders specific to emerging and therapeutically relevant targets (Annunziato *et al.*, 2026; Kwiatkowski *et al.*, 2025; Nicholson *et al.*, 2026; Petzold *et al.*, 2025).

To further resolve distinct conformational states through cryo-EM analysis, Dippon *et al.* (2026) identified an intermediate CRBN state in the presence of an allosteric regulator, SB-405483, and lenalidomide. In this intermediate state, the thalidomide-binding domain was observed to be positioned between the open and closed states, further confirming the dynamic sampling of various conformational states and a

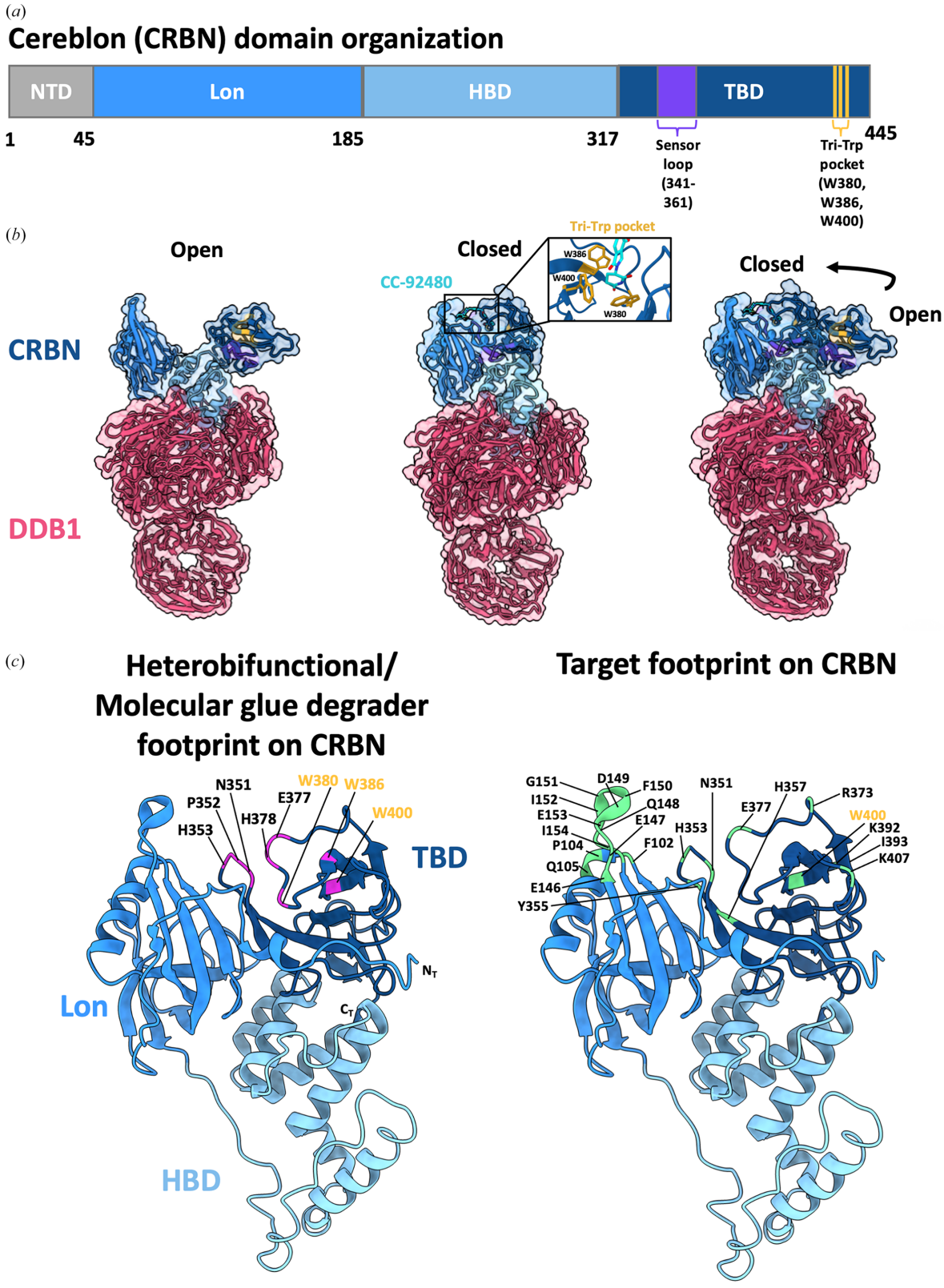


Figure 1
Molecular architecture of cereblon (CRBN) including degrader- and target-binding epitopes. (*a*) Domain organization of CRBN. Lon/NTD, N-terminal domain; HBD, helical bundle domain; TBD, thalidomide-binding domain. (*b*) Surface models from the cryo-EM structures of apo/open (PDB entry 8cvp) and degrader-bound/closed (CC-92480; PDB entry 8d7u) states. The transition from the open to closed form in CRBN–DDB1 is shown. Insets show the tri-Trp pocket (Trp380, Trp 386 and Trp400) in orange and sensor-loop (341–361) residues in purple. (*c*) Heterobifunctional and molecular-glue degrader and target-interacting residues on CRBN from the case studies discussed in this review. Interacting residues highlighted on the CRBN Lon and thalidomide-binding domains from (*b*) are based on PDB-deposited cryo-EM/X-ray crystallographic ternary-complex structures. N_T and C_T denote the N-terminus and C-terminus, respectively. Tri-tryptophan residues are highlighted in yellow.

likely representation of *in situ* states. Altering the equilibrium between open and closed CRBN conformations using orthosteric or allosteric ligands represents an emerging area of research, offering opportunities to structurally and computationally capture transient states and leverage these insights to improve degrader potency (O'Connor *et al.*, 2025). Understanding these various conformational states and how degraders influence the recruitment and degradation of CRBN substrates is becoming increasingly important.

One of the native CRBN substrates, glutamine synthetase (GLUL), identified by Zhao and coworkers, undergoes methylation of the carboxyl group on the C-terminal asparagine by protein carboxymethyltransferase 1 (PCMT1) followed by spontaneous hydrolysis to form the cyclic imide moiety upon stress or aging (Zhao *et al.*, 2026). This was one of the first studies to investigate post-translationally modified sequences (bearing cN or cQ) as native CRBN degrons (Ichikawa *et al.*, 2022). The crystal structure of the minimal degron sequence of GLUL (PFQYKcN) bound to CRBN revealed conserved interactions between the cyclic imide and the tri-Trp pocket and additional molecular contacts between CRBN and residues upstream of the cyclic imide. Direct interactions between GLUL-cN and the CRBN sensor loop increases binding affinity and has direct implications for more efficient substrate ubiquitination and degradation. The structure of CRBN bound to this native degron sequence reaffirms the hypothesis that degraders mimic how native degrons bind to CRBN. While CRBN binds a specific residue-dependent epitope on damaged or enzymatically modified substrates later intended for turnover, degrader-induced binding of CRBN to targets does not have a conserved sequence preference. This has been shown by the uptick in the development of CRBN degraders as therapeutic agents for targets of clinical relevance. This review highlights selected CRBN-recruiting heterobifunctional and molecular-glue degraders and the established importance of structural biology tools in the context of enhancing compound design and efficacy.

2. Structural themes observed in reviewed cases in this article

2.1. Degrader optimization through structure–activity relationship

Characterizing the three-dimensional structures of degrader-mediated ternary complexes has had its challenges, especially as related to deriving the minimal target protein domain required that enables stabilization of the intact complexes for X-ray crystallographic and cryo-EM sample preparation. Molecular-glue degrader-mediated complexes are affected by conformational heterogeneity due to small interaction surface areas (Rui *et al.*, 2023), while heterobifunctional degrader-mediated complexes have complex cooperative dynamics and intrinsic flexibility due to linker composition (Ma *et al.*, 2025). However, the cases reviewed here from Bristol Myers Squibb and Tango Therapeutics show growing possibilities for structurally capturing degrader-mediated CRBN ternary complexes. Here, we discuss a couple of specific examples that illustrate how the determination of high-resolution structures was instrumental in the design and/or validation of the degraders.

2.1.1. BLIMP-1

B-lymphocyte-induced maturation protein 1 (BLIMP-1) is an important transcriptional repressor of genes responsible for the differentiation of mature B cells into antibody-secreting plasma cells (Tang *et al.*, 2022). Multiple myeloma (MM) cells depend on maintenance of the plasma cell state contributed to by constitutive expression of BLIMP-1, which is considered vital for oncogenic survival. Targeted degradation of BLIMP-1 in BLIMP-1 genetically dependent multiple myeloma cells was predicted to negatively affect cellular homeostasis (Shen *et al.*, 2025). As an identified target, Bristol Myers Squibb embarked on a fragment-based discovery of a heterobifunctional degrader that would contain a *de novo* designed BLIMP-1 binder moiety, a CRBN-binding moiety and an optimized linker (Simmons *et al.*, 2025). High-throughput surface plasmon resonance screening identified top BLIMP-1 binders that were structurally characterized by X-ray crystallography to elucidate the molecular interactions between the chemical functional groups and the N-terminal positive regulatory domain. Structural analysis of BLIMP-1 compound 8 identified the solvent-exposed imidazole ring as a suitable 'exit vector' for linker conjugation during degrader development. Compound 8 was altered to include a methylene amine attachment at carbon 7 (C7; of the imidazole group; Fig. 2*a*) that allowed the functionalization of different linkers and cereblon binding moieties. The following compounds were screened by degradation assays, revealing a correlation between degrader potency and carbon chain length (attached at C7). Cellular degradation studies identified compound 18 as an effective degrader, with an EC_{50} of 300 n*M*. Subsequent cryo-EM analysis resolved the ternary complex between BLIMP-1, compound 18 and CRBN, revealing an extensive degrader-mediated protein–protein interface.

Several observations were made from the cryo-EM structure that led to the development of a more potent degrader. Firstly, the attachment of the linker to C7 of the BLIMP-1-binding moiety necessitated an unnecessary bend in the linker to position BLIMP-1 towards CRBN (Fig. 2*a*). This led to linker optimization through shifting the position of the exit vector from the BLIMP-1 binding moiety from C7 to carbon 8 (C8; Fig. 2*b*). This allowed shortening of the linker length (creating compound 21; Fig. 2*b*) while maintaining complex geometry, interface interactions and improving compound efficacy. The cryo-EM structure also showed that the linker weaved through a hydrophobic patch of residues created at the ternary-complex interface and helped to determine additional substituents to improve binding contacts and solubility. These structural insights defined the pharmacophore required for ternary complexation between BLIMP-1 and CRBN and enabled a refined structure–activity relationship to improve the residence time for target ubiquitination, *in vivo* efflux,

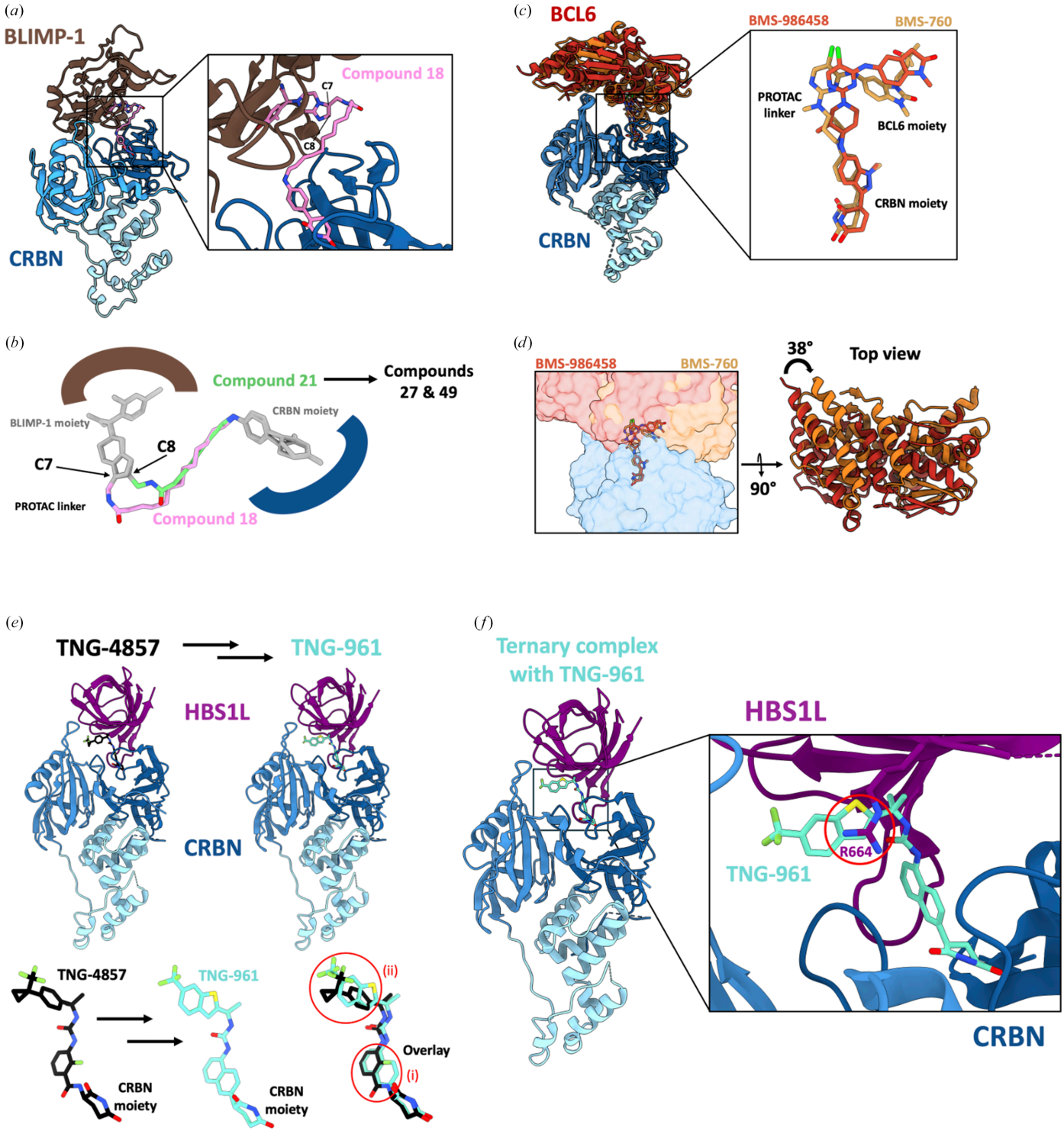


Figure 2
Cereblon degrader potency optimization using structure-based drug design. (*a*) The cryo-EM structure of the ternary complex formed by BLIMP-1 (brown), compound 18 (pink) and CRBN (blue) is shown (PDB entry 9q33). The inset shows the structure and position of the BLIMP-1 targeting heterobifunctional degrader compound 18. Note the linker position change from carbon 7 (C7) to carbon 8 (C8) on the imidazole ring in the BLIMP-1 binding moiety. (*b*) Composition differences in linker chemistry and 3D geometry of compounds 18, 21 and 27 in the optimization series. (*c*) Ternary complex solved by cryo-EM of BCL-6, BMS-986458 (PDB entry 9ya9) or BMS-760 (PDB entry 9q03), and CRBN. The inset shows the comparative positions of both BCL-6 heterobifunctional degraders. (*d*) Surface complementarity of both BCL-6 BTB domain positions in the ternary complex with surface modes shown. The flipped top view shows the shift of the BCL-6 BTB domains relative to each other in the presence of the respective heterobifunctional degraders. (*e*) Cryo-EM structure of HBS1L/GSPT3 in complex with TNG-4857 (PDB entry 11mr) or TNG-961 (PDB entry 10ay) and CRBN. TNG-4857 optimization led to TNG-961, with the bottom panel showing differences in molecular-glue degrader composition and positioning. (i) The fused-ring structure in TNG-961 (cyan) compared with TNG-4857 (black); (ii) the benzothiophene group in the TNG-961 structure (cyan) compared with TNG-4857 (black). (*f*) The inset shows favorable interaction of Arg664 in HBS1L mediated by the benzothiophene group in TNG-961.

Table 1
Summary of CRBN-recruiting heterobifunctional and molecular-glue degraders mentioned in this article.

Residues on CRBN that interact with the corresponding degrader and target protein are given. Only residues mentioned in the respective published research articles are highlighted here. (Tri-Trp pocket: Trp380, Trp386 and Trp400.)

Target protein	Degrader	Disease	Compound stage (clinical trials)	Biopharmaceutical company	Year of release	PDB code	CRBN residues interacting with the MGD/PROTAC	CRBN residues interacting with the neosubstrate	CRBN domain
BLIMP-1	Compound 5 (heterobifunctional degrader)	Multiple myeloma	Preclinical studies	Bristol Myers Squibb	2025	9q33 (cryo-EM)	Tri-Trp pocket, hydrophobic residues which restrict introduction of polar residues groups into the linker	Hydrophobic residues which line the ternary complex interface and restrict introduction of polar groups into the linker	Lon and thalidomide-binding domain
BCL-6	BMS-760 (heterobifunctional degrader)	B-cell non-Hodgkin lymphoma	Preclinical research tool compound	Bristol Myers Squibb	2025	9q03 (cryo-EM)	Tri-Trp pocket, Asn351, Pro352, Glu377, His378	Gln148, Asp149, Phe150, Gly151, Arg373, Glu377	Lon and thalidomide-binding domain
BCL-6	BMS-986458 (heterobifunctional degrader)	B-cell non-Hodgkin lymphoma	Phase I/II (06090539)	Bristol Myers Squibb	2026	9ya9 (cryo-EM)	Tri-Trp pocket, Asn351, Pro352, Glu377, His378	Gln148, Gln148, Phe150, Gly151, Arg373	Lon and thalidomide-binding domain
HBS1L/GSPT3	TNG-4857 (molecular-glue degrader)	FOCAD-deleted cancers (NSLSC, pancreatic *etc.*)	Preclinical research tool compound	Tango Therapeutics	2026	11mr (cryo-EM)	Tri-Trp pocket, His353, Glu377	Asn351, Tyr355, His357, Glu377, Val388, His397, Trp400 (similar to GSPT1–CC-885–CRBN complex)	Lon and thalidomide-binding domain
HBS1L/GSPT3	TNG-961 (molecular-glue degrader)	FOCAD-deleted cancers (NSLSC, pancreatic *etc.*)	IND-enabling studies, entering Phase I	Tango Therapeutics	2026	10ay (cryo-EM)	Tri-Trp pocket, His353, Glu377	Asn351, Tyr355, His357, Glu377, Val388, His397, Trp400 (similar to GSPT1–CC-885–CRBN complex)	Lon and thalidomide-binding domain
VAV1	MRT-6160 (molecular-glue degrader)	Inflammatory diseases (SLE, Sjogren's disease, rheumatoid arthritis, IBD *etc.*)	Phase I trials (0659799), poised to enter Phase II	Monte Rosa, Novartis	2024	9nfr (X-ray crystallography)	Tri-Trp pocket, His353	Lys407	Lon and thalidomide-binding domain
G3BP2	MRT-5702(D) (molecular-glue degrader)	G3BP2-related cancers (breast, lung *etc.*), neurodegenerative diseases	Preclinical research tool compound	Monte Rosa	2025	9os2 (cryo-EM)	Tri-Trp pocket	Asn351, His357, Trp400	Sensor loop and thalidomide-binding domain
CDK2–cyclin-E1	Compound 4 (heterobifunctional degrader)	CCNE-1 amplified and overexpressed cancers	Preclinical research tool compound	Kymera Therapeutics	2025	9d0x (cryo-EM)	Tri-Trp pocket, His353	Pro104, Gln105, Asp149, Phe150, Ile152, His353, Tyr355	Lon and thalidomide-binding domain

permeability and stability (Fan *et al.*, 2025). The lead compound, compound 27, displayed prolonged degradation of BLIMP-1 both on oral and intravenous delivery but was potentially affected by dedifferentiation of plasma cells back to naïve B-cells in multiple myeloma models and not cellular apoptosis. Nevertheless, the efficacy of using structural tools for improvement of degrader design as established by this study contributes to the expanding potential of targeted degradation approaches for transcription factors, proteins that are otherwise considered 'undruggable'.

2.1.2. BCL6

Another degrader design campaign, also pursued by Bristol Myers Squibb, was for a related and well known B-cell differentiation transcription factor, BCL6. Transcription or translational dysregulation of BCL6 expression has been linked to non-Hodgkin's lymphoma, with specific subtypes including diffuse large B-cell lymphoma and follicular lymphoma (Mortensen *et al.*, 2026; Shunatona *et al.*, 2025). BCL6 has therefore been identified as a key target for degradation to eliminate intrinsic and scaffolding functionality, as explored by various biopharmaceutical companies (Pearce *et al.*, 2021; Arvinas Inc./National Institutes of Health, Clinical Trial NCT06393738, 2024). In the initial degrader design against BCL6, researchers started with a BCL6 targeting moiety published by Boehringer Ingelheim, to which they tethered exploratory linkers and cereblon-binding moiety combinations at the piperadine ring (Kerres *et al.*, 2017). One of the initial heterobifunctional degraders (compound 3) yielded an EC_{50} of 5 n*M* that was further optimized to 0.8 n*M* through structure–activity relationship expansion of the BCL6-binding moiety, linker and cereblon-binding moiety to yield the BMS-760 compound (Shunatona *et al.*, 2025). Cryo-EM of two BCL6 monomers in complex with BMS-760 and CRBN demonstrated a large interaction interface with several electrostatic interactions between the proteins and the degrader (Fig. 2*c*).

While BMS-760 displayed a favorable chemotype for ternary-complex formation and cellular degradation, a high oral dose was required to achieve 90% degradation of BCL6, pointing towards low oral bioavailability of this now-tool compound. In a follow-up publication, the Bristol Myers Squibb team further optimized BMS-760 by decreasing the hydrophobicity of the molecule and exploring isomer substitutions leading to the development of BMS-986458, a current Phase I/II clinical trial candidate for non-Hodgkin's lymphoma (National Institutes of Health, Clinical Trial NCT06090539, 2023; Mortensen *et al.*, 2026). The binding affinity of this molecule and its cellular degradation efficiency were comparable to those of BMS-760, yet it afforded a remarkable difference at the ternary-complex interface as indicated by a cryo-EM structure. Although the changes in the surface area of the protein–protein interactions at the complex interface and major interacting residues remained unperturbed compared with the BMS-760 interface (Table 1), the BCL6 broad-complex, tramtrack and bric-à-brac (BTB) domain was shifted by 38° (Fig. 2*d*). This variation in BCL6 position relative to CRBN (Fig. 2*d*) was induced by alterations in linker and BCL6 binding moiety composition and accommodated by the greater flexibility of the Lon domain loop in CRBN. These structures highlight the utility of high-resolution structural studies to understand the architectural flexibility in degrader-induced ternary complexes which have implications for ubiquitination abilities and defining degradation profiles.

2.1.3. HBS1L (also known as GSPT3)

High-resolution cryo-EM and X-ray crystallographic structures have helped guide the design of degraders alike, but are often used as end-stage tools to validate structure–activity hypotheses. Molecular-glue degrader development is complicated compared with that of heterobifunctional degraders due to the necessity of a complementary binding interface, and most molecular-glue discovery pipelines rely on serendipitous discovery through *in vitro* and cellular high-throughput library screens (Kozicka, 2025). This is a separate effort from target identification but requires the same application of high-throughput screening methods. One company that has used this approach is Tango Therapeutics, which developed and optimized an HBS1-like translation GTPase (HBS1L)/GSPT3 degrader (Nicholson *et al.*, 2026). HBS1L was uncovered through a synthetic lethal screen on focadhesion (FOCAD)-deleted cancers with co-deletions of methylthioadenosine phosphorylase (MTAP) and cyclin-dependent kinase inhibitor 2 (CDKN2A). Knockdown of the HBS1L protein in FOCAD-deleted (but not FOCAD-positive) cell models led to the disruption of translational homeostasis and growth inhibition due to removal of the HBS1L/PELO ribosome rescue pathway. To explore this weakness, an in-cell HiBiT-induced proximity assay was used to screen a library of molecular-glue degraders and led to the identification of a potential binder and degradation inducer, TNG-6266. HBS1L/GSPT3 shares sequence homology with GSPT1, a well characterized CRBN target, but TNG-6266 showed selective degradation of HBS1L. TNG-6266 was modified (cereblon-binding moiety and functional group expansion) to TNG-4857, leading to an improved cellular degradation profile. Cryo-EM of TNG-4857 with HBS1L and CRBN revealed molecular-glue flexibility and opportunities to improve interface interactions by coordinating specific glue-interacting residues (Fig. 2*e*). As suggested by structural analyses, the authors rigidified TNG-4857 through the cyclization of several key positions and performed other cellular structure–activity relationship studies leading to the development of TNG-961. The use of a fused-ring system in TNG-961 [labelled (i) in Fig. 2*e*] increased compound rigidity at the cost of entropy but introduced a new electrostatic interaction [labeled (ii) in Fig. 2*e*] between the benzothiophene group in the molecular-glue degrader and the guanidinium group of Arg664 of HBS1L (cation–π stacking; Fig. 2*f*). This case study provides a glimpse into how high-throughput screening and cryo-EM-guided drug design can direct medicinal chemistry to improve degrader potency and selectivity.

2.2. Using ternary-complex structures to explain degrader specificity

As with any other small molecule, degrader molecules display off-target profiles in cells, including off-target binding and/or degradation. This is usually identified through mass spectrometry, but structural tools can also be integrated into the process to understand exhibited compound selectivity. Most studies employing CRRN-recruiting degraders focus on the off-target profiles that involve well known targets (IKZF1, IKZF3, SALL4 *etc*.) due to the conserved phthalimide–glutarimide CRBN-binding moiety (Winter *et al.*, 2015). Although structural studies can highlight areas for selectivity optimization of degraders, we focus here on those using structures of the ternary complexes to explain selectivity.

2.2.1. HBS1L (also known as GSPT3)

The first case study using structural biology to define degrader selectivity comes from the same publication disclosing TNG-961, where Tango Therapeutics also used cryo-EM as a tool to explain TNG-961 degradation specificity for HBS1L (Nicholson *et al.*, 2026). Unlike TNG-961, the GSPT1 degrader CC-885 can induce degradation of GSPT1 and HBS1L/GSPT3 as an off-target effect (Matyskiela *et al.*, 2016). Structural comparison of the ternary complexes (between CRBN–TNG-961–HBS1L and CRBN–CC-885–GSPT1; Fig. 3*a*) shows a similar footprint of the target proteins since both proteins contain the canonical G-loop motif (Sievers, Petzol *et al.*, 2018). However, overlaying the two ternary complexes together provides an explanation for the selectivity of TNG-961. CC-885 fits both binding pockets, but evident steric clashes exist for TNG-961 with GSPT1, specifically with the *gem*-dimethyl and trifluorobenzothiophene groups of TNG-961 (Fig. 3*b*). Specificity of TNG-961 towards HBS1L was also confirmed by showing that GSPT1 was not ubiquitinated (*in vitro* ubiquitination assays), not complexed with CRBN (HiBiT assays), nor degraded (immunoblotting and whole proteome mass spectrometry) in cells. This demonstrates one example where structure is used to explain potency and selectivity characteristics that are required in degraders to push compounds further into the clinical pipeline.

2.2.2. CDK2

Another interesting example is the development of cyclin-dependent kinase 2 (CDK2)-targeting heterobifunctional degraders by Kymera Therapeutics (Collier *et al.*, 2025; Kwiatkowski *et al.*, 2025). Developing traditional ATP-competitive inhibitors poses selectivity challenges due to the highly conserved nature of ATP-binding pockets, especially amongst the cyclin-dependent kinase family of proteins (Łukasik *et al.*, 2021). This provides an opportunity for the development of orthogonal, noncatalytic, binding-pocket ligands for degrader development to eliminate all main and auxiliary protein functions (Burslem *et al.*, 2018). In the study reported by Kymera Therapeutics, the CDK2 binding moiety was first developed and optimized through medicinal chemistry expansion from several existing CDK2 inhibitors to develop compound 2 (Kwiatkowski *et al.*, 2025). The X-ray crystallographic structure of compound 2 with phospho-CDK2 (pCDK2) identified the solvent-exposed portion of the molecule as a sulfonyl group for conjugation of the linker and following cereblon-binding moiety. Following up on multiple iterative rounds of *in silico* prediction, chemical synthesis and cellular activity assays, compound 4 was identified as the lead molecule and a cryo-EM structure was determined of the ternary complex between pCDK2, compound 4 and CRBN (Fig. 3*c*). The ternary-complex structure revealed multiple auxiliary contacts between CDK2 and CRBN in addition to the common interactions seen in degrader-induced complexes. Similar to GSPT1/3, the ternary-complex interface residues between CDK2 and CRBN are sequence-specific and are not conserved amongst other CDK enzymes. When comparing the degrader-induced ternary structures of CDK2–CRBN with a previously deposited inhibitor-bound crystal structure of CDK1, a clear difference in surface topology and electrostatics is observed that sterically precludes CDK1 from complexing with CRBN and compound 4 (Fig. 3*d*). The ternary-complex structure also showed interactions between the Ile205 backbone carbonyl of cyclin-E1 (forms a heterodimer with CDK2 and is co-recruited to the ternary complex) and Lys407 of CRBN. Cyclin-E1 solely binds CDK2, making this another mechanism of selectivity over CDK1. These structural prerequisites indicate that compound 4 selectively binds CDK2 when both cyclin-bound and phosphorylated in cells, providing an explanation for the temporal selectivity seen in the cellular assays. This work further underscores the need for the structural validation of biologically relevant forms of target proteins to understand and build degrader selectivity profiles.

2.2.3. VAV1

Monte Rosa Therapeutics have pioneered a *de novo* target-identification pipeline for molecular-glue degrader discovery using AI- and physics-based algorithms that has led to the development of several drug candidates in clinical trials or as pre-clinical tool compounds, including a VAV1-targeting degrader, MRT-23227, and a G3BP2-targeting degrader, MRT-5702.

VAV guanine nucleotide-exchange factor 1, VAV1, is a key regulator in T- and B-cell signaling and exhibits tissue-specific expression in hematopoietic cells, lowering the potential for off-target effects (Neurath & Berg, 2024). VAV1 was identified through structural similarity to the canonical β-hairpin G-loop found on target proteins bound to degraders and CRBN; specifically, the C-terminal VAV1 Src homology 3 (SH3) domain containing the RT-loop shows significant surface similarity to the canonical G-loop in previously identified CRBN targets (Petzold *et al.*, 2025). Using high-throughput nanoBRET (bioluminescence resonance energy transfer) library screening, several molecular-glue degrader candidates were identified which promoted ternary-complex formation between CRBN and VAV1. From the disclosed results in the publication and patent (McAllister *et al.*, 2024), compound 6

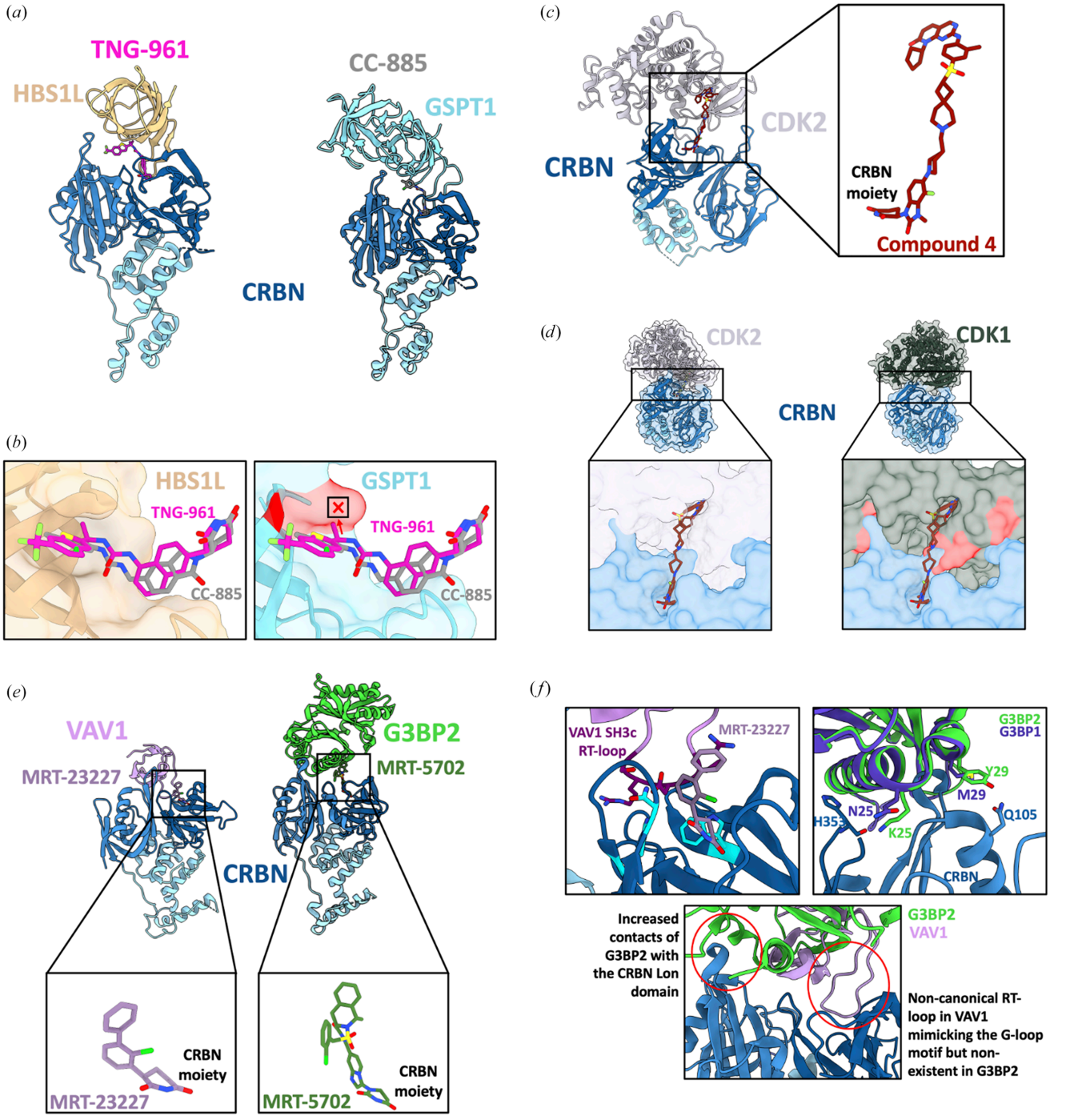


Figure 3
Using structural biology to explain the specificity of CRBN-recruiting heterobifunctional and molecular-glue degraders. (*a*) Structure of TNG-961 bound to HBS1L/GSPT3 (PDB entry 10ay) compared with CC-885 (PDB entry 5hxb) bound to GSPT1. (*b*) Insets show comparison of HBS1L and GSPT1 degraders in the presence of either HBS1L or GSPT1 (CRBN not shown in insets). The red X in the second inset shows clashes of TNG-961 with GSPT1, providing proof of TNG-961 selectivity for HBS1L degradation. (*c*) Cryo-EM of the ternary-complex structure resulting from CDK2–cyclin-E1, compound 4 and CRBN (cyclin-E1 not shown; PDB entry 9d0x). The inset shows the position of compound 4 (CDK2-recruiting heterobifunctional degrader) at the ternary-complex interface. (*d*) Surface model comparison of degrader-bound CDK2 compared with clashes observed between inhibitor-bound CDK1 and CRBN (PDB entry 4y72) to explain heterobifunctional degrader specificity. Cyclin and ribbon models for proteins are not shown here for ease of visualization. (*e*) X-ray crystallographic ternary-complex structure of VAV1, MRT-23227 and CRBN (PDB entry 9nfr). Cryo-EM ternary-complex structure of G3BP2, MRT-5702 and CRBN (PDB entry 9os2). Insets show the position and structure of the respective degraders. A partial MRT-23227 degrader structure is shown due to compound flexibility preventing complete structural elucidation. (*f*) Inset showing the VAV1 SH3c RT-loop in complex with MRT-23227 and CRBN to highlight key interactions in the RT-loop of VAV1 (dark purple) with residues in CRBN (cyan) which are absent in other SH3-domain containing proteins. The inset for G3BP2 and G3BP1 shows residues of G3BP2 (green) which favor ternary-complex formation through specific CRBN residues (for example Q105) compared with G3BP1 (purple). The bottom panel shows differences in G3BP2 and VAV1 recruitment to CRBN via the respective degraders through noncanonical structural motifs and surface complementarity.

(also known as MRT-23227) was identified as the top hit for CRBN engagement that demonstrated 93.34% degradation of VAV1 in cells with a DC_{50} (half-maximal degradation concentration) of 7.35 n*M* VAV1 (and not VAV2 or VAV3) in cells. The disclosure from the company indicates that the final clinical candidate they nominated, MRT-6160 (National Institutes of Health, Clinical Trial NCT06597799, 2024), had a comparable 97% degradation of VAV1 with a DC_{50} of 7 n*M* (compound 185 in the patent). The ternary structure of MRT-6160 in complex with VAV1-SH3c and CRBN was not published, but the crystal structure of the ternary complex with MRT-23227 was released (Fig. 3*e*). Interactions between CRBN and the VAV1 SH3c were mediated by several residues (Ser799, Asp797 and Arg796), matching what was computationally predicted (Fig. 3*f*). The VAV1-SH3c domain exhibits sequence divergence amongst the VAV homologs, specifically at the key interacting residues important for ternary-complex formation with the degrader. Mutagenesis experiments and whole-proteome mass-spectrometry studies demonstrated the high level of specificity that MRT-23227 has towards VAV1. Most degrader-mediated interactions occur between the compound and CRBN, except for Arg796 on VAV1, which contributes to cation–π stacking interactions with the terminal ring in the degrader (Fig. 3*f*). Other SH3 domain-containing proteins in the proteome (∼300 proteins; Kazlauskas *et al.*, 2016) have poor sequence homology with VAV1-SH3c, and those with similar residues lack the necessary coordinating residues required for ternary-complex formation with CRBN and the VAV1 degrader.

2.2.4. G3BP2

Using a similar surface analogy prediction tool as that used to identify VAV1, Ras GTPase-activating protein-binding protein 2 (G3BP2) was also identified as another G-loop-independent target for CRBN by Monte Rosa Therapeutics (Annunziato *et al.*, 2026). The cellular screens identified the molecular-glue degrader MRT-5702, which induced CRBN recruitment to G3BP2 and its subsequent degradation with high selectivity. Cryo-EM structures of the MRT-5702-mediated ternary complex demonstrated engagement of the CRBN Lon domain with a specific G3BP2 domain (Fig. 3*e*). This is another noncanonical interaction site as previous degraders mainly interact with the thalidomide-binding domain of CRBN. This was due to the mimicry of CRBN of the native binding partner of G3BP2, USP10, as identified through predictive-structural screening methods developed by Monte Rosa Therapeutics. Other well characterized CRBN-recruiting degraders do not recruit G3BP2 due to this unconventional binding interface, further providing selectivity for the G3BP2 molecular-glue degrader. The structures also revealed selectivity of the degrader for G3BP2 compared with G3BP1 due to sequence divergence at key binding sites (Fig. 3*f*). Specifically, Tyr29 and Lys25 on G3BP2 form hydrogen-bond interactions with Gln105 and His353 on CRBN, whereas the respective positions on G3BP1, Met29 and Asn25, have shorter side chains and are less electro-negative, therefore ablating binding to CRBN. This highly specific electrostatic footprint and surface complementarity at protein–protein interfaces is essential for degrader-induced ternary-complex formation, target ubiquitination and degradation (Fan *et al.*, 2025). This work is an excellent example of how predictive and experimental structural biology can be used to expand the druggable proteome for CRBN with noncanonical structural motifs, inducing new interaction hotspots.

3. Future directions

Targeted protein degradation is a rapidly evolving field, with novel innovations and methods being reported regularly to accelerate the discovery or enhancement of novel chemical moieties. Reviews highlighting advances in high-throughput biophysical screening methods have been documented elsewhere (Casement *et al.*, 2021; Ward *et al.*, 2023; Holdgate *et al.*, 2024; Ponzo *et al.*, 2026; Shaum *et al.*, 2026), but here we discuss how structural biology is being leveraged to understand and improve degrader discovery.

3.1. Visualizing cullin–RING E3 ligase complexes

The crystal and cryo-EM structures discussed in this review focus entirely on how CRBN is engaged by heterobifunctional and molecular-glue degraders, and targets. Information on ubiquitination and proteolytic degradation must however be obtained by nonstructural methods such as *in vitro* and cellular assays. Determining the structures of entire E3 ligase complexes is a monumental challenge as it requires several proteins in specific states, which in the case of CRBN complexes can include target protein and degrader, CRBN, DDB1, CUL4A, RBX1, UbcH5a, Nedd8 and ubiquitin (Sievers, Gasser *et al.*, 2018). Capturing this entire cullin–RING ligase 4 complex requires optimization of recombinant protein production, complexation conditions including overcoming dissociation kinetics, and crystallography or cryo-EM conditions (Crowe & Ciulli, 2026). However, a study by Deng *et al.* (2025) determined the cryo-EM structure of the $CRL4^{CRBN}$–IKZF3 complex with eight molecular-glue degraders, revealing not only the protein–protein interface between CRBN, the degrader and the target protein, but also how the E2 and ubiquitin are associated. This structural characterization addresses a key question in CRBN biology of how target binding to CRBN degraders positions lysine residues on the target protein for ubiquitination by the ubiquitin-loaded E2 enzyme (Li *et al.*, 2024). These structures demonstrate that Lys166 on IKZF3 is in proximity to the ubiquitin-loaded E2 enzyme, providing structural evidence for the major ubiquitylation site observed in mass-spectrometric data. In addition to these structures, other groups have published the multimeric structure of another gold-standard E3 ligase, the von Hippel–Lindau (VHL) E3 ligase receptor, in complex with the rest of the proteins constituting the cullin–RING ligase 2 complex (Sternicki *et al.*, 2026). Visualizing E3 ligase complexes by predictive modeling (Bai *et al.*, 2022) or

by experimental structures is a major advance for CRBN biochemistry as it can begin to explain differences in degrader potency in cells.

3.2. Predictive CRBN ternary-complex modeling

With the growing repository of experimentally validated CRBN structures (Zhu *et al.*, 2026), predictive modeling and pattern-recognition software, such as *AlphaFold*3, is becoming increasingly more accurate in predicting novel protein–ligand and protein–protein interactions (Abramson *et al.*, 2024). Companies including Isomorphic Labs are using these AI-based tools as the foundation for their *Isomorphic Drug Discovery Engine* (*IsoDDE*) that has been used to identify cryptic binding sites on CRBN (Isomorphic Labs Team, 2026), consistent with the structural studies of the allosteric regulator SB-405483 reported by Dippon *et al.* (2026). Insilico Medicine has also employed predictive AI algorithms to generate targeted protein-degradation moieties, including a heterobifunctional degrader that targets PKMYT1, a cytoplasmic membrane-associated serine–threonine protein kinase (Wang *et al.*, 2025). The predicted CRBN–degrader–PKMYT1 ternary complexes were modeled into a predicted cullin–RING ligase 4 complex and the degraders were further optimized to position surface-exposed lysine residues on PKMYT1 for ubiquitination and were able to display nanomolar binding to both CRBN and PKMYT1. While some experimental data will always be required to optimize the drug-like properties of the hit molecule, these approaches potentially eliminate the need for extensive organic synthesis campaigns and high-throughput library screens, thus accelerating the discovery of degraders.

4. Conclusion

CRBN has become one of the most well known proteins in targeted protein degradation, specifically arising from structural studies and serendipitous discoveries of small-molecule binders. Structural biology has become an increasingly useful tool to advance candidates from proof-of-concept tools to valuable medicines, while with the advent of AI-based platforms for *in silico* small-molecule screening (Lv *et al.*, 2025), the degrader and target discovery space has exponentially grown over the past few years (Zhang *et al.*, 2026). Companies such as Bristol Myers Squibb and Kymera Therapeutics have used structural biology to demonstrate how heterobifunctional degrader linkers can be optimized to maximize target engagement and selectivity, maximizing cellular degradation potency. Likewise, companies such as Tango Therapeutics and Monte Rosa Therapeutics have used crystal and cryo-EM structures to explain perceived degrader selectivity and to perform structure-guided compound optimization. Looking to the future, advances in capturing entire E3 ligase complexes and AI-based predictive modeling can be expected to reduce the time to discovery of CRBN degraders, not just for pharmaceutical companies but also in academic research laboratories. The predictive advances in structural biology pertinent to CRBN-degrader technology can potentially extend to all ∼600 E3 ligases (Kozicka, 2025). CRBN, despite its tragic discovery through the use of thalidomide, is now the core modality used in targeted protein degradation and is poised to enable the development of several life-saving drugs.

Acknowledgements

We thank Dr Peter Axerio-Cilies for help with the recapitulation of the BLIMP-1 heterobifunctional degrader pose. We would also like to thank the numerous researchers in the cereblon targeted protein-degradation field who are not mentioned explicitly in the main text or in the references.

Conflict of interest

The authors declare no conflicts of interest.

Data availability

No data were used for the research described in the article.

Funding information

This work was supported by awards to Sriram Subramaniam from a Canada Excellence Research Chair Award and the VGH Foundation. SA was supported by a University of British Columbia (UBC) Four Year Doctoral Fellowship.

References

Abramson, J., Adler, J., Dunger, J., Evans, R., Green, T., Pritzel, A., Ronneberger, O., Willmore, L., Ballard, A. J., Bambrick, J., Bodenstein, S. W., Evans, D. A., Hung, C.-C., O'Neill, M., Reiman, D., Tunyasuvunakool, K., Wu, Z., Žemgulytė, A., Arvaniti, E., Beattie, C., Bertolli, O., Bridgland, A., Cherepanov, A., Congreve, M., Cowen-Rivers, A. I., Cowie, A., Figurnov, M., Fuchs, F. B., Gladman, H., Jain, R., Khan, Y. A., Low, C. M. R., Perlin, K., Potapenko, A., Savy, P., Singh, S., Stecula, A., Thillaisundaram, A., Tong, C., Yakneen, S., Zhong, E. D., Zielinski, M., Žídek, A., Bapst, V., Kohli, P., Jaderberg, M., Hassabis, D. & Jumper, J. M. (2024). *Nature*, **630**, 493–500.

Annunziato, S., Quan, C., Donckele, E. J., Lamberto, I., Bunker, R. D., Zlotosch, M., Schwander, L., Murthy, A., Wiedmer, L., Staehly, C., Matysik, M., Gilberto, S., Kapsitidou, D., Wible, D., De Donatis, G. M., Trenh, P., SriRamaratnam, R., Strande, V., Lieberherr, R., Lyon, D., Steiner, D., Silva, J., Almeida, R., Dolgikh, E., DeMarco, B., Tsai, J., Sadok, A., Zarayskiy, V., Walter, M., Tiedt, R., Lumb, K. J., Bonenfant, D., Fasching, B., Castle, J. C., Townson, S. A., Gainza, P. & Petzold, G. (2026). *Nat. Struct. Mol. Biol.* **33**, 479–487.

Asatsuma-Okumura, T., Ando, H., De Simone, M., Yamamoto, J., Sato, T., Shimizu, N., Asakawa, K., Yamaguchi, Y., Ito, T., Guerrini, L. & Handa, H. (2019). *Nat. Chem. Biol.* **15**, 1077–1084.

Bai, N., Riching, K. M., Makaju, A., Wu, H., Acker, T. M., Ou, S.-C., Zhang, Y., Shen, X., Bulloch, D. N., Rui, H., Gibson, B. W., Daniels, D. L., Urh, M., Rock, B. M. & Humphreys, S. C. (2022). *J. Biol. Chem.* **298**, 101653.

Békés, M., Langley, D. R. & Crews, C. M. (2022). *Nat. Rev. Drug Discov.* **21**, 181–200.

Burslem, G. M., Smith, B. E., Lai, A. C., Jaime-Figueroa, S., McQuaid, D. C., Bondeson, D. P., Toure, M., Dong, H., Qian, Y., Wang, J., Crew, A. P., Hines, J. & Crews, C. M. (2018). *Cell Chem. Biol.* **25**, 67–77.

Campone, M., De Laurentiis, M., Jhaveri, K., Hu, X., Ladoire, S., Patsouris, A., Zamagni, C., Cui, J., Cazzaniga, M., Cil, T., Jerzak,

K. J., Fuentes, C., Yoshinami, T., Rodriguez-Lescure, A., Sezer, A., Fontana, A., Guarneri, V., Molckovsky, A., Mouret-Reynier, M.-A., Demirci, U., Zhang, Y., Valota, O., Lu, D. R., Martignoni, M., Parameswaran, J., Zhi, X., Hamilton, E. P. & VERITAC-2 Study Group (2025). *N. Engl. J. Med.* **393**, 556–568.
Casement, R., Bond, A., Craigon, C. & Ciulli, A. (2021). *Methods Mol. Biol.* **2365**, 79–113.
Chamberlain, P. P., Lopez-Girona, A., Miller, K., Carmel, G., Pagarigan, B., Chie-Leon, B., Rychak, E., Corral, L. G., Ren, Y. J., Wang, M., Riley, M., Delker, S. L., Ito, T., Ando, H., Mori, T., Hirano, Y., Handa, H., Hakoshima, T., Daniel, T. O. & Cathers, B. E. (2014). *Nat. Struct. Mol. Biol.* **21**, 803–809.
Collier, P. N., Zheng, X., Ford, M., Weiss, M., Chen, D., Li, K., Growney, J. D., Yang, A., Sathappa, M., Breitkopf, S. B., Enerson, B., Liang, T., Paul, A., Sawant, R., Su, L., Aversa, R. J., Howarth, C., Sharma, K., Williams, J. & Kwiatkowski, N. P. (2025). *J. Med. Chem.* **68**, 18407–18422.
Crowe, C. & Ciulli, A. (2026). *Chem. Rev.* **126**, 5755–5791.
Deng, Z., Ai, H., Shi, Q., Liang, J., He, Z., Zheng, J., Li, H., Zhang, L., He, W., Tao, S., Zheng, Q., He, W., Pan, M. & Liu, L. (2025). *bioRxiv*, 2025.06.08.658527.
Dippon, V. N., Rizvi, Z., Choudhry, A. E., Chung, C., Alkuraya, I. F., Xu, W., Tao, X. B., Jurewicz, A. J., Schneck, J. L., Chen, W., Curnutt, N. M., Kabir, F., Chan, K.-H., Queisser, M. A., Musetti, C., Dai, H., Lander, G. C., Benowitz, A. B. & Woo, C. M. (2026). *Nature*, **651**, 482–490.
Donovan, K. A., An, J., Nowak, R. P., Yuan, J. C., Fink, E. C., Berry, B. C., Ebert, B. L. & Fischer, E. S. (2018). *eLife*, **7**, e38430.
Fan, A. T., Gadbois, G. E., Huang, H., Chaudhry, C., Jiang, J., Sigua, L. H., Smith, E. R., Wu, S., Poirier, G. J., Dunne–Dombrink, K., Goyal, P., Tao, A. J., Sellers, W. R., Fischer, E. S., Donovan, K. A. & Ferguson, F. M. (2025). *Angew. Chem. Int. Ed.* **64**, e202417272.
Fischer, E. S., Böhm, K., Lydeard, J. R., Yang, H., Stadler, M. B., Cavadini, S., Nagel, J., Serluca, F., Acker, V., Lingaraju, G. M., Tichkule, R. B., Schebesta, M., Forrester, W. C., Schirle, M., Hassiepen, U., Ottl, J., Hild, M., Beckwith, R. E. J., Harper, J. W., Jenkins, J. L. & Thomä, N. H. (2014). *Nature*, **512**, 49–53.
Holdgate, G. A., Bardelle, C., Berry, S. K., Lanne, A. & Cuomo, M. E. (2024). *SLAS Discov.* **29**, 100136.
Ichikawa, S., Flaxman, H. A., Xu, W., Vallavoju, N., Lloyd, H. C., Wang, B., Shen, D., Pratt, M. R. & Woo, C. M. (2022). *Nature*, **610**, 775–782.
Isomorphic Labs Team (2026). *Accurate Predictions of Novel Biomolecular Interactions with IsoDDE*. https://10.5281/zenodo.19699685.
Ito, T., Ando, H., Suzuki, T., Ogura, T., Hotta, K., Imamura, Y., Yamaguchi, Y. & Handa, H. (2010). *Science*, **327**, 1345–1350.
Kazlauskas, A., Schmotz, C., Kesti, T., Hepojoki, J., Kleino, I., Kaneko, T., Li, S. S. C. & Saksela, K. (2016). *Mol. Cell. Proteomics*, **15**, 3270–3281.
Kerres, N., Steurer, S., Schlager, S., Bader, G., Berger, H., Caligiuri, M., Dank, C., Engen, J. R., Ettmayer, P., Fischerauer, B., Flotzinger, G., Gerlach, D., Gerstberger, T., Gmaschitz, T., Greb, P., Han, B., Heyes, E., Iacob, R. E., Kessler, D., Kölle, H., Lamarre, L., Lancia, D. R., Lucas, S., Mayer, M., Mayr, K., Mischerikow, N., Mück, K., Peinsipp, C., Petermann, O., Reiser, U., Rudolph, D., Rumpel, K., Salomon, C., Scharn, D., Schnitzer, R., Schrenk, A., Schweifer, N., Thompson, D., Traxler, E., Varecka, R., Voss, T., Weiss-Puxbaum, A., Winkler, S., Zheng, X., Zoephel, A., Kraut, N., McConnell, D., Pearson, M. & Koegl, M. (2017). *Cell Rep.* **20**, 2860–2875.
Kozicka, Z. (2025). *Essays Biochem.* **69**, 379–391.
Kwiatkowski, N., Liang, T., Sha, Z., Collier, P. N., Yang, A., Sathappa, M., Paul, A., Su, L., Zheng, X., Aversa, R., Li, K., Mehovic, R., Kolodzy, C., Breitkopf, S. B., Chen, D., Howarth, C. L., Yuan, K., Jo, H., Growney, J. D., Weiss, M. & Williams, J. (2025). *Cell Chem. Biol.* **32**, 556–569.
Li, J., Purser, N., Liwocha, J., Scott, D. C., Byers, H. A., Steigenberger, B., Hill, S., Tripathi-Giesgen, I., Hinkle, T., Hansen, F. M., Prabu, J. R., Radhakrishnan, S. K., Kirkpatrick, D. S., Reichermeier, K. M., Schulman, B. A. & Kleiger, G. (2024). *Mol. Cell*, **84**, 1304–1320.
Łukasik, P., Baranowska-Bosiacka, I., Kulczycka, K. & Gutowska, I. (2021). *Int. J. Mol. Sci.* **22**, 2806.
Lv, W., Jia, X., Tang, B., Ma, C., Fang, X., Jin, X., Niu, Z. & Han, X. (2025). *Eur. J. Med. Chem.* **289**, 117432.
Ma, N., Bhattacharya, S., Muk, S., Jandova, Z., Schmalhorst, P. S., Ghosh, S., Le, K., Diers, E., Trainor, N., Farnaby, W., Roy, M. J., Kofink, C., Greb, P., Weinstabl, H., Ciulli, A., Bader, G., Sankar, K., Bergner, A. & Vaidehi, N. (2025). *Nat. Commun.* **16**, 8595.
Matyskiela, M. E., Clayton, T., Zheng, X., Mayne, C., Tran, E., Carpenter, A., Pagarigan, B., McDonald, J., Rolfe, M., Hamann, L. G., Lu, G. & Chamberlain, P. P. (2020). *Nat. Struct. Mol. Biol.* **27**, 319–322.
Matyskiela, M. E., Couto, S., Zheng, X., Lu, G., Hui, J., Stamp, K., Drew, C., Ren, Y., Wang, M., Carpenter, A., Lee, C.-W., Clayton, T., Fang, W., Lu, C.-C., Riley, M., Abdubek, P., Blease, K., Hartke, J., Kumar, G., Vessey, R., Rolfe, M., Hamann, L. G. & Chamberlain, P. P. (2018). *Nat. Chem. Biol.* **14**, 981–987.
Matyskiela, M. E., Lu, G., Ito, T., Pagarigan, B., Lu, C.-C., Miller, K., Fang, W., Wang, N.-Y., Nguyen, D., Houston, J., Carmel, G., Tran, T., Riley, M., Nosaka, L., Lander, G. C., Gaidarova, S., Xu, S., Ruchelman, A. L., Handa, H., Carmichael, J., Daniel, T. O., Cathers, B. E., Lopez-Girona, A. & Chamberlain, P. P. (2016). *Nature*, **535**, 252–257.
McAllister, L. A., Liardo, E., Ritzén, A., Oleinikovas, V., Lucas, X., Fasching, B., Bizzini, L. D. & Lesieur, M. (2024). Patent WO2024151547A1.
Mortensen, D. S., Shunatona, H. P., Holmberg-Douglas, N., Rhodes, J., Da Silva, D., Gamez, J., Groza, M., Zhu, J., Christoforou, A., Johnson, S. A., Khambatta, G., Narla, R. K., Nimje, R. Y., Huang, D., Dodd, D. S., Griffin, J., Miseo, G., Whitefield, B., Weiss, D. R., Rader, J., Kuzu, E., Leisten, J., Lai, C., Shi, L., Del Rosario, J., Dalvie, D., Rolfe, M., Zapf, C. W., Belmont, P., Alexander, M., Bence, N. & Groocock, L. (2026). *J. Med. Chem.* **69**, 4424–4438.
Neurath, M. F. & Berg, L. J. (2024). *Trends Immunol.* **45**, 580–596.
Nicholson, H. E., Whittington, D. A., Bruzzese, F. J., Lazarides, K., Martires, L. C. M., Tonini, M. R., Jenkins, H. N., Zhang, M., Shahagadkar, P., Pratt, C. B., Briggs, K. J., McCarren, P., Tsai, A., Bandi, M., Min, C., Huang, A., Zhang, H., Meier, S. R., Shen, B., Yu, Y., Liang, C., Liu, Y., Teng, T., Zhang, J., Crystal, A., Mallender, W. D., Wu, X. E., Maxwell, J. P. & Andersen, J. N. (2026). *Cancer Discov.* **16**, 1884–1902.
Nowak, R. P., DeAngelo, S. L., Buckley, D., He, Z., Donovan, K. A., An, J., Safaee, N., Jedrychowski, M. P., Ponthier, C. M., Ishoey, M., Zhang, T., Mancias, J. D., Gray, N. S., Bradner, J. E. & Fischer, E. S. (2018). *Nat. Chem. Biol.* **14**, 706–714.
O'Connor, S., Rutter, Z. J., Cowan, A. D., Zeeb, M., Binder, F., Cao, Y., Chakraborti, S., Djukic, S., Geist, L., Hogg, E., Kidd, G., Krumb, M., Langer, S., Schmidt, D., Martin, L., McCrory, E. H., Padroni, G., Puoti, I., Simpson, L., Sturbaut, M., Crozier, L., Vetma, V., Zhang, Q., McAulay, K., Theis, T. & Ciulli, A. (2025). *bioRxiv*, 2025.12.19.695617.
Pearce, A. C., Bamford, M. J., Barber, R., Bridges, A., Convery, M. A., Demetriou, C., Evans, S., Gobbetti, T., Hirst, D. J., Holmes, D. S., Hutchinson, J. P., Jayne, S., Lezina, L., McCabe, M. T., Messenger, C., Morley, J., Musso, M. C., Scott-Stevens, P., Manso, A. S., Schofield, J., Slocombe, T., Somers, D., Walker, A. L., Wyce, A., Zhang, X.-P. & Wagner, S. D. (2021). *J. Biol. Chem.* **297**, 100928.
Petzold, G., Fischer, E. S. & Thomä, N. H. (2016). *Nature*, **532**, 127–130.
Petzold, G., Gainza, P., Annunziato, S., Lamberto, I., Trenh, P., McAllister, L. A., DeMarco, B., Schwander, L., Bunker, R. D., Zlotosch, M., SriRamaratnam, R., Gilberto, S., Langousis, G., Donckele, E. J., Quan, C., Strande, V., De Donatis, G. M., Alabi, S. B., Alers, J., Matysik, M., Staehly, C., Dubois, A., Osmont, A., Garskovas, M., Lyon, D., Wiedmer, L., Oleinikovas, V., Lieberherr, R., Rubin, N. T., Lam, D. T., Lucas, X., Liardo, E., Widlund, N. I., Ritzén, A., Caceres, R. M., Vigil, D., Tsai, J., Wallace, O., Peluso, M., Sadok, A., Tiedt, R., Paterson, A. M., Zarayskiy, V., Fasching, B.,

Bonenfant, D., Warmuth, M., Castle, J. C. & Townson, S. A. (2025). *Science*, **389**, eadt6736.
Ponzo, I., Soldà, A., Crowe, C., Dahl, G., Jahodová, T., Heerwig, A., Geschwindner, S., Ciulli, A. & Rant, U. (2026). *ACS Sens.* **11**, 3876–3888.
Rui, H., Ashton, K. S., Min, J., Wang, C. & Potts, P. R. (2023). *RSC Chem. Biol.* **4**, 192–215.
Shaum, J. B., Muñoz, I., Ordoño, M., Steen, E. A., Wenge, D. V., Cheong, H., Janowski, J., Hunkeler, M., Bilotta, E. M., Rutter, Z. J., Barta, P. A., Thornhill, A. M., Milosevich, N., Hargis, L. M., Bishop, T. R., Carter, T. R., da Camara, B., Hinterndorfer, M., Dada, L., He, W.-J., Offensperger, F., Furihata, H., Schweber, S. R., Hatton, C., Wen, Y., Cravatt, B. F., Engle, K. M., Donovan, K. M., Melillo, B., Kitamura, S., Ciulli, A., Armstrong, S. A., Fischer, E. S., Winter, G. E. & Erb, M. A. (2026). *Nat. Chem. Biol.* **22**, 1540–1552.
Shen, M., Sharma, A., Andersen, C., Nelson, J., Debreczeni, J., Hauke, P., Wu, M., Huang, Y., Dillman, K., Liang, H., Liu, Z., Tokheim, C., Seong, A., Chan, L., Moreau, K., Seneviratne, U., Singh, M., Quinn, T., Morrill, L., Davies, R., Gutierrez, P., Srivastava, A., Voulgarelis, D., Lamb, M., Saeh, J., Younes, A., Wilson, D., Fawell, S., Drew, L. & Tavana, O. (2025). *Blood*, **146**, 2554–2554.
Shunatona, H. P., Holmberg Douglas, N., Rhodes, J., Thomas, W., Da Silva, D., Gamez, J., Groza, M., Christoforou, A., Zhu, J., Johnson, S., Dodd, D., Huang, D., Griffin, J., Miseo, G., Whitefield, B., Weiss, D., Rader, J., Kuzu, E., Leisten, J., Del Rosario, J., Shi, L., Matyskiela, M., Chamberlain, P. P., Belmont, P., Alexander, M., Zapf, C. W., Groocock, L. & Mortensen, D. S. (2025). *J. Med. Chem.* **68**, 21502–21519.
Sievers, Q. L., Gasser, J. A., Cowley, G. S., Fischer, E. S. & Ebert, B. L. (2018). *Blood*, **132**, 1293–1303.
Sievers, Q. L., Petzold, G., Bunker, R. D., Renneville, A., Słabicki, M., Liddicoat, B. J., Abdulrahman, W., Mikkelsen, T., Ebert, B. L. & Thomä, N. H. (2018). *Science*, **362**, eaat0572.
Simmons, B. J., Groocock, L., Moreno, J., Peters, D. S., Hughes, M. E., Veeravalli, V., Crawford, J. M., Chalkley, M., Griffith, M., Plooster, M., Hu, B., Gamez, J., Leisten, J., Barnes, M. J., Chinn, J., Deb, G., Modi, H., Katepalli, M., Weiss, D., Won, W., Sun, Z., Yu, S., Reid, C., Donnell, A. F., Li, L., Watson, E. R., Perrin-Ninkovic, S., Shi, L., Narla, R. K., Zapf, C. W., Bence, N., Lopez-Girona, A. & Riggs, J. R. (2025). *J. Med. Chem.* **68**, 25385–25402.
Sternicki, L. M., Crowe, C., Wieske, L. H. E., Ciulli, A. & Poulsen, S.-A. (2026). *Anal. Chem.* **98**, 20377–20388.
Stewart, M. D., Ritterhoff, T., Klevit, R. E. & Brzovic, P. S. (2016). *Cell Res.* **26**, 423–440.
Tang, T. F., Chan, Y. T., Cheong, H. C., Cheok, Y. Y., Anuar, N. A., Looi, C. Y., Gan, G. G. & Wong, W. F. (2022). *Cell Immunol.* **380**, 104594.
Wang, Y., Wang, X., Liu, T., Wang, C., Meng, Q., Meng, F., Yu, J., Liu, J., Fan, Y., Gennert, D., Pun, F. W., Aliper, A., Ren, F., Zhang, M., Cai, X., Ding, X. & Zhavoronkov, A. (2025). *Nat. Commun.* **16**, 10759.
Ward, J. A., Perez–Lopez, C. & Mayor–Ruiz, C. (2023). *ChemBioChem*, **24**, e202300163.
Watson, E. R., Novick, S., Matyskiela, M. E., de la Chamberlain, P. P. H., Peña, A., Zhu, J., Tran, E., Griffin, P. R., Wertz, I. E. & Lander, G. C. (2022). *Science*, **378**, 549–553.
Winter, G. E., Buckley, D. L., Paulk, J., Roberts, J. M., Souza, A., Dhe-Paganon, S. & Bradner, J. E. (2015). *Science*, **348**, 1376–1381.
Xu, W. & Woo, C. M. (2025). *Acc. Chem. Res.* **58**, 1632–1643.
Zhang, Y., Li, L., Xu, J., Che, C., Jia, J., Lu, H., You, Q. & Xu, X. (2026). *Molecules*, **31**, 459.
Zhao, Z., Xu, W., Feng, E. Y., Cao, S., Hermoso-López, A., Peña-Vega, P., Lloyd, H. C., Porter, A. K. D., Guzmán, M., Zheng, N. & Woo, C. M. (2026). *Nat. Chem. Biol.* **22**, 802–812.
Zhu, J., Liao, Y., Lin, H., Xie, J., Deng, Z., Han, J., Zhang, Z., Xiao, J., Wang, Z., Zhang, S., Lai, L. & Pei, J. (2026). *Nucleic Acids Res.* **54**, D1500–D1509.